

Evidence of rotational autoionization in the threshold region of the photoionization spectrum of CH₃

Maritoni Litorja and Branko Ruscic

Chemistry Division, Argonne National Laboratory, Argonne, Illinois 60439-4831

(Received 1 August 1997; accepted 12 September 1997)

The photoionization spectrum of the threshold region of CH₃ equilibrated at room temperature has been recorded and compared to the zero electron kinetic energy (ZEKE) spectrum of Blush *et al.* [J. Chem. Phys. **98**, 3557 (1993)]. The ionization onset region is at ~ 70 cm⁻¹ higher energy than previous high-temperature photoionization work [Chupka and Lifshitz, J. Chem. Phys. **48**, 1109 (1967)], but still ~ 34 cm⁻¹ lower than that implied by invoking only direct ionization. The residual discrepancy can be accounted for by including fully allowed quadrupole-induced and partially allowed dipole-induced rotational autoionization, thus making the observed onset completely congruous with the ZEKE ionization potential. In addition, the fragment appearance potential of CH₃⁺ from CH₄ was redetermined by accurate fitting as AP₀(CH₃⁺/CH₄) = 14.322 ± 0.003 eV. With the very precise ZEKE ionization potential, this yields the best current value for the bond dissociation energy in methane, D₀(H-CH₃) = 4.484 ± 0.003 eV = 103.40 ± 0.07 kcal/mol (104.96 ± 0.07 kcal/mol at 298 K). © 1997 American Institute of Physics. [S0021-9606(97)03247-9]

I. INTRODUCTION

The methyl radical, produced by pyrolysis of suitable precursors, was examined previously¹ by photoionization at a resolution of ~ 100 cm⁻¹. The threshold region is dominated by a strong 0 ← 0 vibrational Franck-Condon factor, manifesting itself as a “sharp” step with a half-rise at 9.825 ± 0.010 eV. Normally, this value would be interpreted as the adiabatic ionization potential (IP). However, it was ~ 150 cm⁻¹ lower than Herzberg’s spectroscopic determination² of 79 392 ± 5 cm⁻¹ ≡ 9.8434 ± 0.0006 eV, obtained by extrapolating early members of three Rydberg series. Although the general appearance of the photoionization threshold led them to the assumption that autoionization does not occur in the threshold region, Chupka and Lifshitz¹ concluded that the discrepancy must nevertheless be due to an inadequate interpretation of the threshold shape.

Subsequent photoelectron spectroscopic (PES) investigations³⁻⁵ at a resolution of ~ 120 –160 cm⁻¹ yielded³ 9.837 ± 0.005 eV as the adiabatic IP, in reasonable agreement with Herzberg’s value.² More recently,⁶ the ionization threshold region of CH₃ (produced by flash pyrolysis of azomethane) was examined by pulsed field ionization (PFI). The rotationally resolved (~ 1.5 cm⁻¹) spectrum of near-zero kinetic energy electrons (ZEKE) yielded an adiabatic IP of 79 349 ± 3 cm⁻¹ ≡ 9.8380 ± 0.0004 eV, somewhat (43 cm⁻¹) lower than Herzberg’s value² (and in excellent agreement with the coarser PES value³), but still 105 cm⁻¹ higher than the photoionization value.¹

If direct ionization were indeed the only significant contributor to the ionization threshold region of CH₃, then an integral over the PES or ZEKE spectrum should fairly reproduce the threshold shape of the photoionization yield curve. A brief glance at the ZEKE spectrum⁶ suggests that such an integral would tend to produce a relatively simple steplike shape, with the midrise not too far from the position of the

head of the Q branch. The hot rotational distribution of CH₃ (1000–1300 K) in the photoionization experiment¹ is expected to extend the breadth of the branches and thus decrease the slope of the threshold, but should not cause an appreciable net shift to lower energy. Hence, in the absence of autoionization, there appears to be no obvious reason why the midrise of the photoionization step should not yield an IP compatible with PES or PFI.

In this paper we would like to show that the photoionization spectrum of the threshold region of CH₃, when equilibrated at room temperature, yields an ionization onset closer to the ZEKE value⁶ than previous high-temperature photoionization experiments,¹ and demonstrate that the apparent residual discrepancy can be explained by invoking rotational autoionization.

II. EXPERIMENT

The basic instrumentation employed here was recently described elsewhere.⁷ CH₃ was produced *in situ* by hydrogen abstraction from methane. Fluorine atoms were generated in a low-pressure microwave discharge through pure fluorine and piped into a small cuplike region, where they reacted with the methane precursor. The construction of the radical source ensures that species emanating into the ionization region have undergone several collisions with the source walls and are thus equilibrated to ambient temperature. The reaction yield was optimized by manually adjusting the output power of the microwave source and the flows of F₂ and CH₄. The experiments utilized the many-lined Werner and Lyman emission bands of H₂, which provided an accurate internal wavelength calibration.

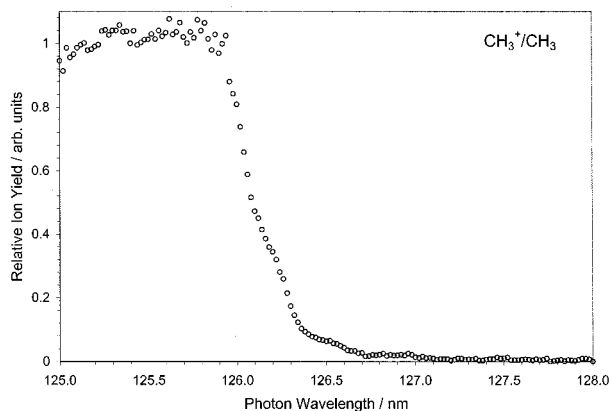


FIG. 1. The threshold region of the photoion yield curve of CH_3 obtained by reaction of CH_4 with F atoms. The radical is equilibrated at room temperature.

III. RESULTS

Figure 1 displays a mass-resolved ($m/e = 15$) scan of the threshold region of CH_3 covering 125–128 nm, recorded at medium resolution ($\sim 50 \text{ cm}^{-1}$), and at 0.02 nm point density. The wavelength scale calibration is believed to be correct to $< 0.01 \text{ nm}$ ($\sim 5 \text{ cm}^{-1}$). The overall shape of the threshold, which corresponds to the vibrationless ($0 \leftarrow 0$) $\text{CH}_3^+ \bar{X}^1A_1' \leftarrow \text{CH}_3, \bar{X}^2A_2''$ transition, is indeed that of a giant step. The nominal midrise position is at $\sim 126.08 \pm 0.02 \text{ nm} \equiv 9.8338 \pm 0.0016 \text{ eV}$, some 70 cm^{-1} higher than the value reported by Chupka and Lifshitz,¹ but still $\sim 34 \text{ cm}^{-1}$ shy of the PFI value.⁶ The plateau region displays muddled autoionization structure converging to higher vibrational levels of the ion, while the ascending portion of the step shows some substructure in the form of gentle steps or undulations. The very weak steplike structure at $\sim 127.02 \pm 0.05 \text{ nm}$ is readily assigned as a ν_2 hot band (a_2'' out-of-plane bend,^{8–10} 606.5 cm^{-1}). Its intensity ($\sim 1\%$) roughly corresponds to room temperature Boltzmann population of ν_2 ($\sim 5\%$), reduced by the $0 \leftarrow 1$ Franck–Condon factor. The stronger $1 \leftarrow 1$ transition falls $\sim 780 \text{ cm}^{-1}$ beyond the threshold.^{4(b),5} The remaining humplike undulations observable in the threshold region (peaking at ~ 126.5 , ~ 126.2 , and perhaps ~ 125.9 – 126.0 nm) are difficult to rationalize via vibrational hot bands.

IV. DISCUSSION

A. Direct ionization in the threshold region

Using known rotational constants^{9,11} of CH_3 and CH_3^+ , we have produced a simple simulation of the relevant rotational structure. The continua accessible from the ground state of $\text{CH}_3, \bar{X}^2A_2''$, consist of the $\text{CH}_3^+ \bar{X}^1A_1'$ ion core coupled to ksa_1', kda_1' , and kde'' outgoing electron channels. These mirror the Rydberg series (β, δ , and γ) observed by Herzberg.² The $ksa_1' \beta^2A_1'$ and $kda_1' \delta^2A_1'$ continua are accessible by parallel, and $kde'' \gamma^2E''$ by perpendicular transitions. The $\Delta J = 0, \pm 1$ selection rule leads to $\Delta N = 0, \pm 1, \pm 2$ ($\Delta K = 0$) for parallel and $\Delta N = 0, \pm 1, \pm 2, \pm 3$ (ΔK

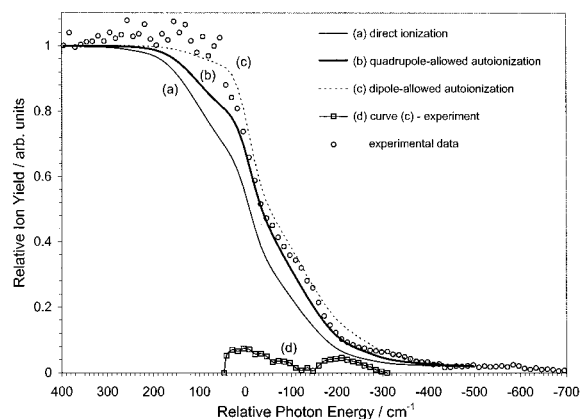


FIG. 2. Various simulations of the shape of the ionization threshold of CH_3 . The energy scale is relative to the adiabatic ionization potential, taken from Ref. 6 as $9.8380 \pm 0.0004 \text{ eV}$. (a) Curve incorporating only direct ionization. (b) Curve incorporating quadrupole-allowed rotational autoionization of $nde'' \gamma^2E''$ Rydberg states. (c) Curve obtained by assuming that, in addition, dipole-induced autoionization is fully allowed. (d) The difference between the experimental data points and curve (c).

$= 0, \pm 2$, as shown by Blush *et al.*⁶) for perpendicular transitions. As manifested by the ZEKE spectrum,⁶ propensity rules tend to emphasize $\Delta N = 0, \pm 1$ transitions. Thus, the simulation uses only P, Q , and R branches, with the addition of a weak O branch. However, it includes both $\Delta K = 0$ and $\Delta K = \pm 2$ subbands, in spite of the fact that Blush *et al.*⁶ state that there is very little indication of the latter. Apparent evidence to the contrary is the line assigned⁶ as R_0 . With only $\Delta K = 0$ available, it would require $N^+ = 1, K^+ = 0$ as the final level, nonexistent by virtue of nuclear spin statistics¹² if CH_3^+ is of D_{3h} symmetry. With $\Delta K = \pm 2$, there are several small lines in the immediate vicinity, accounting for the experimental observation.

The individual line intensities were estimated by taking into account the nuclear spin statistics, degeneracy, and the Boltzmann population of the initial states, as well as the nuclear spin statistics and degeneracy of the ionic states. To simulate the direct ionization portion of the photoionization threshold, the calculated transitions were convoluted with the experimental resolution and integrated. A baseline offset to accommodate the ν_2 hot band was added, and the intensity adjusted to match the relative experimental scale, making some allowance for the autoionization structure in the plateau region. The result is shown in Fig. 2(a), as a thin solid line on an energy scale relative to the ionization potential of Blush *et al.*⁶ ($79349 \pm 3 \text{ cm}^{-1}$). The direct ionization model clearly predicts that the adiabatic IP is near the midrise point. Compared to the experiment, the curve is shifted nonuniformly to higher energy. Thus, one concludes that direct ionization alone is not sufficient to explain the photoionization threshold.

B. Autoionization in the threshold region

The modeling of autoionization phenomena is more intricate. The β, δ , and γ Rydberg states converging to every

rotational level of the ion can autoionize if the appropriate (i.e., the same symmetry, parity, and total angular momentum) continuum and mechanism is available. Since CH_3^+ does not have a permanent dipole moment, only quadrupole ($\Delta N^+ = \text{even}$) autoionization will be fully allowed. While the $nsa'_1 \beta^2 A'_1$ and $nda'_1 \delta^2 A'_1$ Rydberg states are not capable of autoionizing via this mechanism, the $nde'' \gamma^2 E''$ Rydberg states have two J values in common with the kde'' continuum built upon the $N^+ - 2$ level. The partial cross section associated with these Rydberg states will appear as an autoionizing quasicontinuum, producing a miniature steplike contribution to the ion yield with an onset at the $N^+ - 2$ level of the ion. Without autoionization, the corresponding contribution would have had an onset at N^+ level. The simulation that includes autoionization from the appropriate J space of $nde'' \gamma^2 E''$ Rydberg states is depicted in Fig. 2(b) (the thick solid line). The curve grazes the experimental points from the high-energy side and appears to account for the bulk of the observed threshold shape, missing only the additional intensity present in the regions of the three humps mentioned in Sec. III. Rather than at the midrise, the adiabatic IP is now located closer to the upper end of the step.

The $nsa'_1 \beta^2 A'_1$ and $nda'_1 \delta^2 A'_1$ Rydberg states have one J value in common with both the ksa'_1 and kda'_1 continuum channels built upon the $N^+ - 1$ level of the ion, while the $nde'' \gamma^2 E''$ Rydberg states have three J values in common with the analogous kde'' continuum. In addition, the γ Rydberg states also have one J value in common with the kde'' continuum built upon the $N^+ - 3$ level of the ion. Thus, if a dipole mechanism were available, one-half of the J space of β and δ Rydberg states and three-quarters of the J space of γ Rydberg states with appropriate n^* values could autoionize. If fully allowed, such autoionization could make the S (and T) rotational branches unavailable to ZEKE-type experiments, which rely on time-delayed pulsed-field ionization of very high n^* Rydberg states. However, in the O , P , Q , and R branches there is a significant number of J values for which autoionization is not possible. These nonautoionizing states are sufficient to comfortably reproduce the line positions and approximately the intensities measured by Blush *et al.*⁶

The assumption that the dipole mechanism is fully operating produces the simulation depicted in Fig. 2(c) (dashed line). Not surprisingly, this curve overestimates the ion yield, grazing the data on the low-energy side. The experimental trace could now be perceived as if it consisted of curve (c) with the addition of broad valleys, shown inverted by subtracting the experimental data from curve (c), Fig. 2(d). One valley is centered at -210 cm^{-1} , with perhaps two additional poorly resolved valleys at -90 and 0 cm^{-1} . The structure is obscured at the high-energy side partly by the (vibrational) autoionization occurring in the plateau region in the experiment, and partly by the fact that the R branch is slightly overemphasized in the simulation. The position of the valleys coarsely resembles an unresolved rotational spectrum shifted to lower energy by $\sim 90\text{--}120 \text{ cm}^{-1}$.

One potentially active dipole mechanism can be traced to the dipole induced by the repeller field, which is always

present in photoionization mass spectrometric experiments. In this case one would expect to see a dependence on the magnitude of the repeller field. To explore this aspect, we have recorded spectra at various repeller settings, ranging from 0.8 to 12.5 V/cm. Within the statistical uncertainty of the data, all spectra appeared identical. Another possible candidate is the momentary dipole that occurs as CH_3^+ undergoes the zero-point out-of-plane vibrational motion. This dipole will not be very efficient in inducing autoionization, since, in classical terms, its vibrational period is about three orders of magnitude shorter than the orbital period of an $n^* \approx 50$ Rydberg electron. On the other hand, its efficiency has to be compared to the lifetime of the Rydberg states in the absence of autoionization, which can be substantial. However marginal, such a mechanism will be more efficient for low Rydberg states (with shorter orbital periods), and will become less effective as n^* increases. This n^* dependence will change the shape of the contribution to the ion yield. Instead of a flattop step, the contribution will now display an onset corresponding to lower n^* states, followed by a depression and regaining intensity close to the ionization limit. The depression corresponds to the Rydberg states with intermediate n^* values, for which this mechanism is inefficient. Very high n^* states, close to the ionization limit, can autoionize via an induced dipole mechanism even in weak fields, since their polarizability increases as n^6 . A similar overall effect, albeit related to induced-dipole autoionization, has been postulated previously for N_2 .¹³ The anticipated cumulative effect of such depressions in the partial ionization cross sections is to create broader spectral valleys preceding the onsets of the principal rotational branches.

The modeling of partially allowed dipole-induced autoionization, whether by a mechanism similar to the one described above or some other, would be a tall task even with the aid of sophisticated quantum mechanical calculations capable of yielding the proper n^* dependence of autoionization probability. However, in order to qualitatively test the plausibility of the ideas outlined above, we have performed exploratory simulations which incorporated quenching of dipole-allowed autoionization for intermediate n^* values in a very crude manner. These tests suggested that such quenching effects could indeed lead to a structured threshold shape with broad valleys roughly in the appropriate positions.

Overall, the simulations shown in Fig. 2 demonstrate that the bulk of the photoionization threshold shape can be explained by direct ionization via a weak O branch and normally developed P , Q , and R branches, combined with quadrupole-induced autoionization of $nde'' \gamma^2 E''$ Rydberg states. The additional structure in the experimental spectrum is probably caused by partially allowed dipole-induced ionization of all three ($nsa'_1 \beta^2 A'_1$, $nda'_1 \delta^2 A'_1$, and $nde'' \gamma^2 E''$) Rydberg series converging to the threshold. The implication of the autoionization model is that the selection of the midrise of the threshold step as adiabatic IP is not appropriate in this case. Instead, the proper value is close to the high end of the step. However, the traditional shortcut, which selects the midrise of the threshold step as the adiabatic IP (and thus effectively ignores rotational substructure

even if only direct ionization were present), would in practice lead to a relatively small error (for thermodynamic purposes) of $0.0042 \text{ eV} = 34 \text{ cm}^{-1} = 0.10 \text{ kcal/mol}$.

The described threshold effects involving autoionization are ultimately thermal in their nature, inasmuch as their intensity is derived from the Boltzmann population of rotational levels of the initial neutral species. As mentioned in Sec. I, if only direct ionization were present, the enhanced temperatures would simply extend the breadth of the branches and thus decrease the slope of the threshold, without causing an appreciable net shift of the midrise to lower energy. However, rotational autoionization builds up intensity below the nominal threshold(s). While the magnitude of the resulting departure from the simple midrise interpretation is small to moderate at room temperature, it is expected to be substantially larger at elevated temperatures, such as used previously.¹

With the autoionization model proposed here, the room-temperature photoionization experiment becomes completely compatible with the precise adiabatic IP value of $9.8380 \pm 0.0004 \text{ eV}$ obtained by Blush *et al.*⁶ If, instead, the spectroscopic value² of $9.8434 \pm 0.0006 \text{ eV}$ is used in the modeling, a much poorer fit to the data is obtained. Compared to Fig. 2, the simulated curves appear shifted to higher energy to the extent that even the full inclusion of dipole-induced autoionization still substantially underestimates the experimental data, clearly indicating that this IP value is too high.

C. Thermodynamical consequences

Herzberg's extrapolated value² for $\text{IP}(\text{CH}_3)$, quoted¹⁴ as $9.843 \pm 0.002 \text{ eV}$, and a photoionization measurement¹⁵ of the appearance potential (AP) of the CH_3^+ fragment from CH_4 , $\text{AP}_0(\text{CH}_3^+/\text{CH}_4) = 14.320 \pm 0.004 \text{ eV}$, which lead to $D_0(\text{H}-\text{CH}_3) = 103.2 \pm 0.1 \text{ kcal/mol}$, are the basis for the currently recommended¹⁴ values $D_0(\text{H}-\text{CH}_3) = 103.3 \pm 0.1 \text{ kcal/mol}$ and $\Delta H_f^0{}_{298}(\text{CH}_3) = 35.0 \pm 0.1 \text{ kcal/mol}$. Using the PFI value⁶ for $\text{IP}(\text{CH}_3)$ instead of Herzberg's, introduces a slight variance of $\sim 0.12 \text{ kcal/mol}$. However, most of this shift ($\sim 0.09 \text{ kcal/mol}$) can be compensated for by using the alternate determination of $\text{AP}_0(\text{CH}_3^+/\text{CH}_4) = 14.324 \pm 0.003 \text{ eV}$ by McCulloh and Dibeler;¹⁶ which appears to be at least as reliable as Chupka's.¹⁵ In view of the two slightly different determinations of $\text{AP}(\text{CH}_3^+/\text{CH}_4)$, we have decided to reexamine the fragment yield curve of CH_3^+ from CH_4 and use our recently developed fitting procedures^{7,17} to either confirm or amend the appearance potential. A full account of the fitting procedure used here has been given recently elsewhere.⁷ Figure 3 shows the experimental data recorded at 300 K and the fit, barely discernible from the points, as well as the implied ion yield curve corresponding to 0 K. The derived AP at 0 K is $14.322 \pm 0.003 \text{ eV}$, in very good agreement (within the respective error bars) with both previous determinations,^{15,16} and, in fact, it coincides with their arithmetic average.

With the PFI-ZEKE value $\text{IP}(\text{CH}_3) = 9.8380 \pm 0.0004 \text{ eV}$, which appears to be fully supported by the present study, our redetermined $\text{AP}_0(\text{CH}_3^+/\text{CH}_4)$

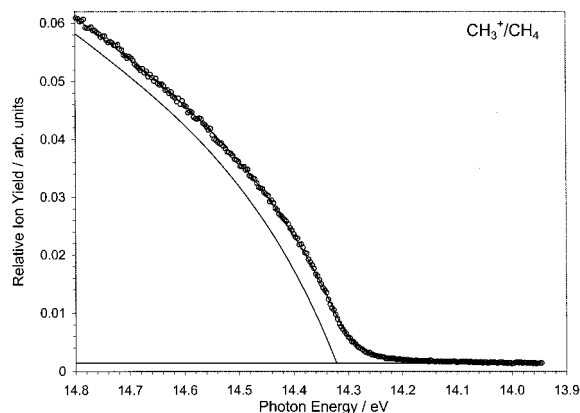


FIG. 3. The photon yield curve of the CH_3^+ fragment from methane. The solid line barely discernible under the experimental points is a model fit at the experimental temperature (300 K), while the line displaced toward higher energy is the derived fragment ion yield at 0 K. The fitted value for the appearance potential is $\text{AP}_0(\text{CH}_3^+/\text{CH}_4) = 14.322 \pm 0.003 \text{ eV}$.

$= 14.322 \pm 0.003 \text{ eV}$ yields the best current value for the bond dissociation energy in methane of $D_0(\text{H}-\text{CH}_3) = 4.484 \pm 0.003 \text{ eV} = 103.40 \pm 0.07 \text{ kcal/mol}$ ($104.96 \pm 0.07 \text{ kcal/mol}$ at 298 K), only a shade higher than the most recent recommendation.¹⁴ With auxiliary heats of formation,¹⁸ this translates into $\Delta H_f^0{}_{0}(\text{CH}_3) = 35.84 \pm 0.09 \text{ kcal/mol}$ and $\Delta H_f^0{}_{298}(\text{CH}_3) = 35.03 \pm 0.09 \text{ kcal/mol}$. The corresponding heat of formation of the CH_3^+ ion is $\Delta H_f^0{}_{0}(\text{CH}_3^+) = 262.71 \pm 0.09 \text{ kcal/mol}$.

V. CONCLUSION

Earlier photoionization work¹ on the methyl radical, which was generated by pyrolysis of dimethyl mercury and/or methyl nitrate at 1000–1300 K, implies an adiabatic IP that is lower than the PFI-ZEKE determination⁶ by 105 cm^{-1} . When CH_3 is equilibrated at room temperature, the ionization onset region appears $\sim 70 \text{ cm}^{-1}$ closer to the PFI-ZEKE value. However, a simple interpretation of the threshold shape that includes only direct ionization, still produces an apparent discrepancy of $\sim 34 \text{ cm}^{-1}$. The residual disparity can be accounted for by including fully allowed quadrupole-induced and partially allowed dipole-induced rotational autoionization. This makes the observed photoionization onset completely congruous with the ZEKE ionization potential⁶ of $9.8380 \pm 0.0004 \text{ eV}$, and indicates that Herzberg's extrapolated value² of $9.8434 \pm 0.0006 \text{ eV}$ is slightly too high. The autoionization model also helps rationalize why the ionization onset of thermally hot CH_3 appears to be depressed when compared to other data.

In addition, the fragment appearance potential of CH_3^+ from CH_4 was redetermined by accurate fitting as $\text{AP}_0(\text{CH}_3^+/\text{CH}_4) = 14.322 \pm 0.003 \text{ eV}$. With the very precise ZEKE ionization potential, this yields the best current value for the bond dissociation energy in methane, $D_0(\text{H}-\text{CH}_3) = 4.484 \pm 0.003 \text{ eV} = 103.40 \pm 0.07 \text{ kcal/mol}$ ($104.96 \pm 0.07 \text{ kcal/mol}$ at 298 K).

ACKNOWLEDGMENT

This work was supported by the U.S. Department of Energy, Office of Basic Energy Sciences, under Contract No. W-31-109-ENG-38.

- ¹W. A. Chupka and C. Lifshitz, *J. Chem. Phys.* **48**, 1109 (1967).
²G. Herzberg, *Proc. R. Soc. London, Ser. A* **262**, 291 (1961).
³L. Golob, N. Jonathan, A. Morris, M. Okuda, and K. J. Ross, *J. Electron Spectrosc. Relat. Phenom.* **1**, 506 (1972/73).
⁴(a) T. Koenig, T. Balle, and W. Snell, *J. Am. Chem. Soc.* **97**, 662 (1975);
(b) T. Koenig, T. Balle, and J. C. Chang, *Spectrosc. Lett.* **9**, 755 (1976).
⁵J. Dyke, N. Jonathan, E. Lee, and A. Morris, *J. Chem. Soc. Faraday 2* **72**, 1385 (1976).
⁶J. A. Blush, P. Chen, R. T. Wiedman, and M. G. White, *J. Chem. Phys.* **98**, 3557 (1993).
⁷R. L. Asher, E. H. Appelman, and B. Ruscic, *J. Chem. Phys.* **105**, 9781 (1996).
⁸M. E. Jacox, *Vibrational and Electronic Energy Levels of Polyatomic Transient Molecules* [*J. Phys. Chem. Ref. Data, Monogr.* **3**, (1994)].
⁹C. Yamada, E. Hirota, and K. Kawaguchi, *J. Chem. Phys.* **75**, 5256 (1981).
¹⁰J. Wormhoudt and K. E. McCurdy, *Chem. Phys. Lett.* **156**, 47 (1989).
¹¹M. W. Crofton, M.-F. Jagod, B. D. Rehfuss, W. A. Kreiner, and T. Oka, *J. Chem. Phys.* **88**, 666 (1988).
¹²G. Herzberg, *Molecular Spectra and Molecular Structure. II. Infrared and Raman Spectra of Polyatomic Molecules* (Krieger, Malabar, FL, 1991).
¹³J. Berkowitz and B. Ruscic, *J. Chem. Phys.* **93**, 1741 (1990); see also B. Ruscic and J. Berkowitz, *ibid.* **93**, 1747 (1990).
¹⁴J. Berkowitz, G. B. Ellison, and D. Gutman, *J. Phys. Chem.* **98**, 2744 (1994).
¹⁵W. A. Chupka, *J. Chem. Phys.* **48**, 2337 (1968).
¹⁶K. E. McCulloh and V. H. Dibeler, *J. Chem. Phys.* **64**, 4445 (1976).
¹⁷(a) B. Ruscic and J. Berkowitz, *J. Phys. Chem.* **97**, 11451 (1993); (b) *J. Chem. Phys.* **100**, 4498 (1994); (c) **101**, 7795 (1994); (d) **101**, 7975 (1994); (e) **101**, 10936 (1994); (f) R. L. Asher and B. Ruscic, *ibid.* **106**, 210 (1997).
¹⁸(a) L. V. Gurvich, I. V. Veyts, and C. B. Alcock, *Thermodynamic Properties of Individual Substances* (Hemisphere, New York, 1989), Vol. 1, Parts 1 and 2; (b) *Thermodynamic Properties of Individual Substances* (Hemisphere, New York, 1991), Vol. 2, Parts 1 and 2.